Supporting Information for

The role of Arctic sea ice loss in the interdecadal trends of the East Asian summer monsoon in a warming climates

Xiaoqi Zhang[1,2], Bian He[2*], Qing Bao[2*], Yimin Liu[2,3], Guoxiong Wu[2,3], Anmin Duan[4], Wenting Hu[2], Chen Sheng[2], Jian Rao[1]

[1] Key Laboratory of Meteorological Disaster, Ministry of Education (KLME) / Joint International Research Laboratory of Climate and Environment Change (ILCEC) / Collaborative Innovation Center on Forecast and Evaluation of Meteorological Disasters (CIC-FEMD), Nanjing University of Information Science and Technology, Nanjing 210044, China.

[2] State Key Laboratory of Numerical Modeling for Atmospheric Sciences and Geophysical Fluid Dynamics (LASG), Institute of Atmospheric Physics, Chinese Academy of Sciences, Beijing, 100029.

[3] College of Earth and Planetary Sciences, University of Chinese Academy of Sciences, Beijing, 100049.

[4] State Key Laboratory of Marine Environmental Science, College of Ocean and Earth Sciences, Xiamen University, Xiamen, 361005.

Contents of this file:

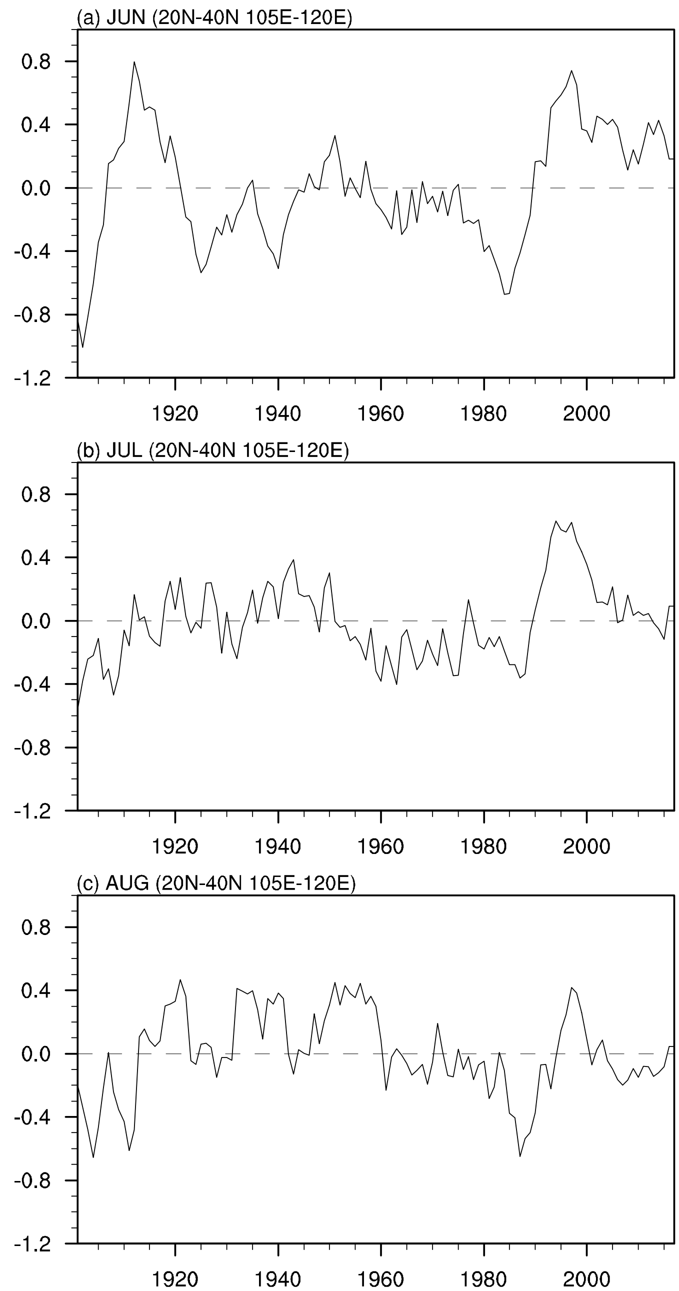

Supplementary Figure 1. Regional average precipitation in East Asia. Regional average precipitation (20°N-40°N, 105°E-120°E) in East Asia from 1901 to 2017 (mm day^{-1}).

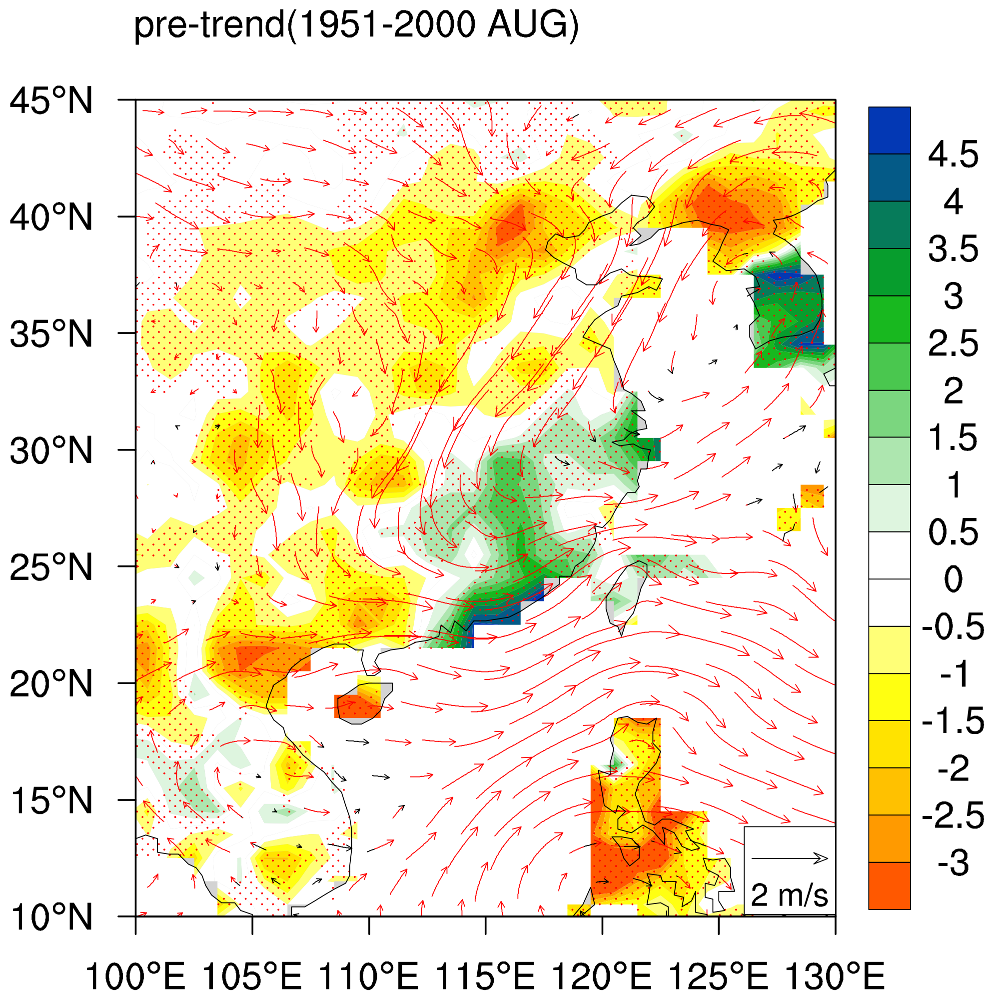

Supplementary Figure 2. Trends of precipitation and 850 hPa wind in August. Precipitation (shading, units: mm day^{-1}) and 850hPa wind (vector, units: m s^{-1}) trends in August for GPCC/ERA5 during 1951-2000. Stippling and red vectors indicate where the trends or the multi-model ensemble mean response is significant (90% confidence).

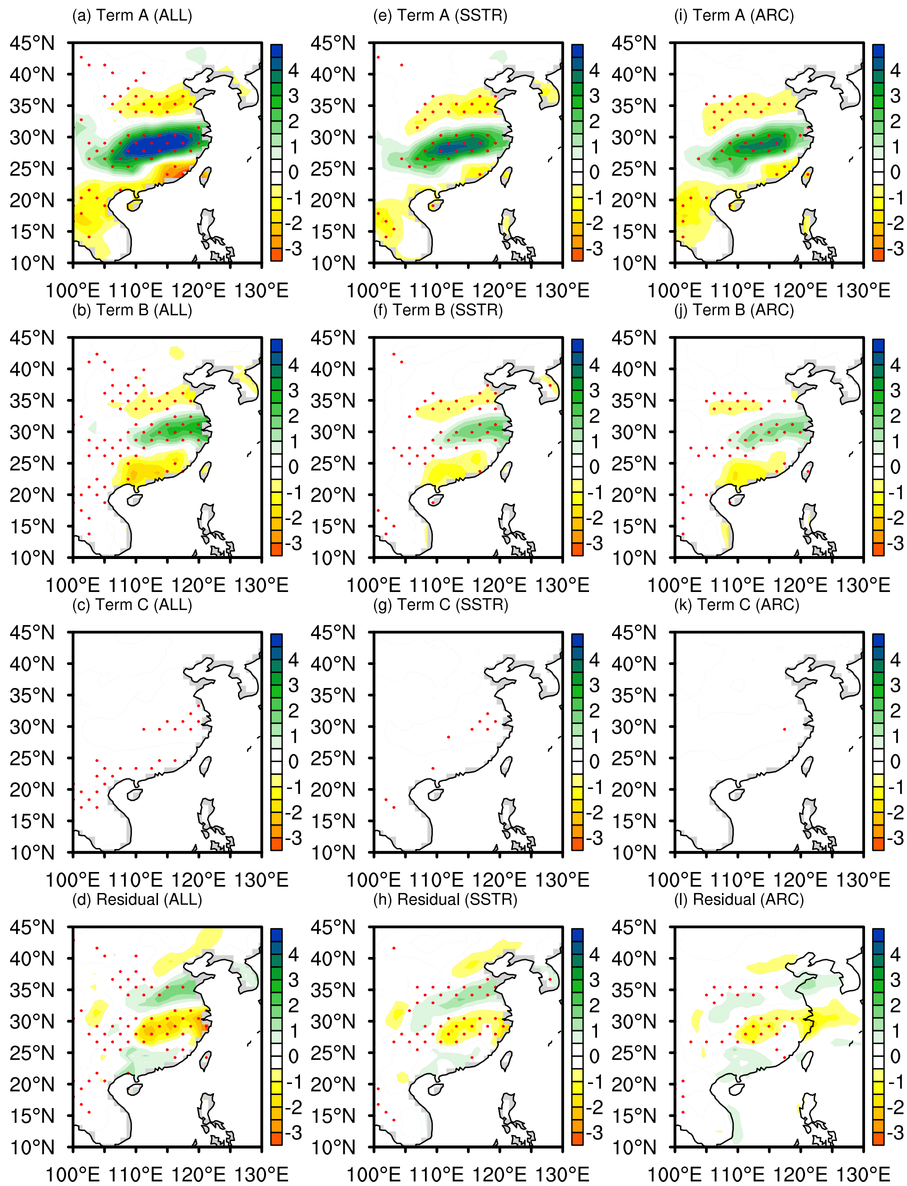

Supplementary Figure 3. Moisture processes driving changes in precipitation anomaly (June). The vertical transport differences of water vapor ($-\langle \omega \partial_p q \rangle'$, units: mm day^{-1}) responses to ALL (a), SSTR (e) and ARC (i). The horizontal transport differences of water vapor ($-\langle \mathbf{V}_h \cdot \nabla_h q \rangle'$, units: mm day^{-1}) responses to ALL (b), SSTR (f) and ARC (j). The evaporation (E', units: mm day^{-1}) responses to ALL (c), SSTR (g) and ARC (k). The residual (δ', units: mm day^{-1}) responses to ALL (d), SSTR (h) and ARC (l). Stippling indicates where the multi-model ensemble mean response is significant (90% confidence).

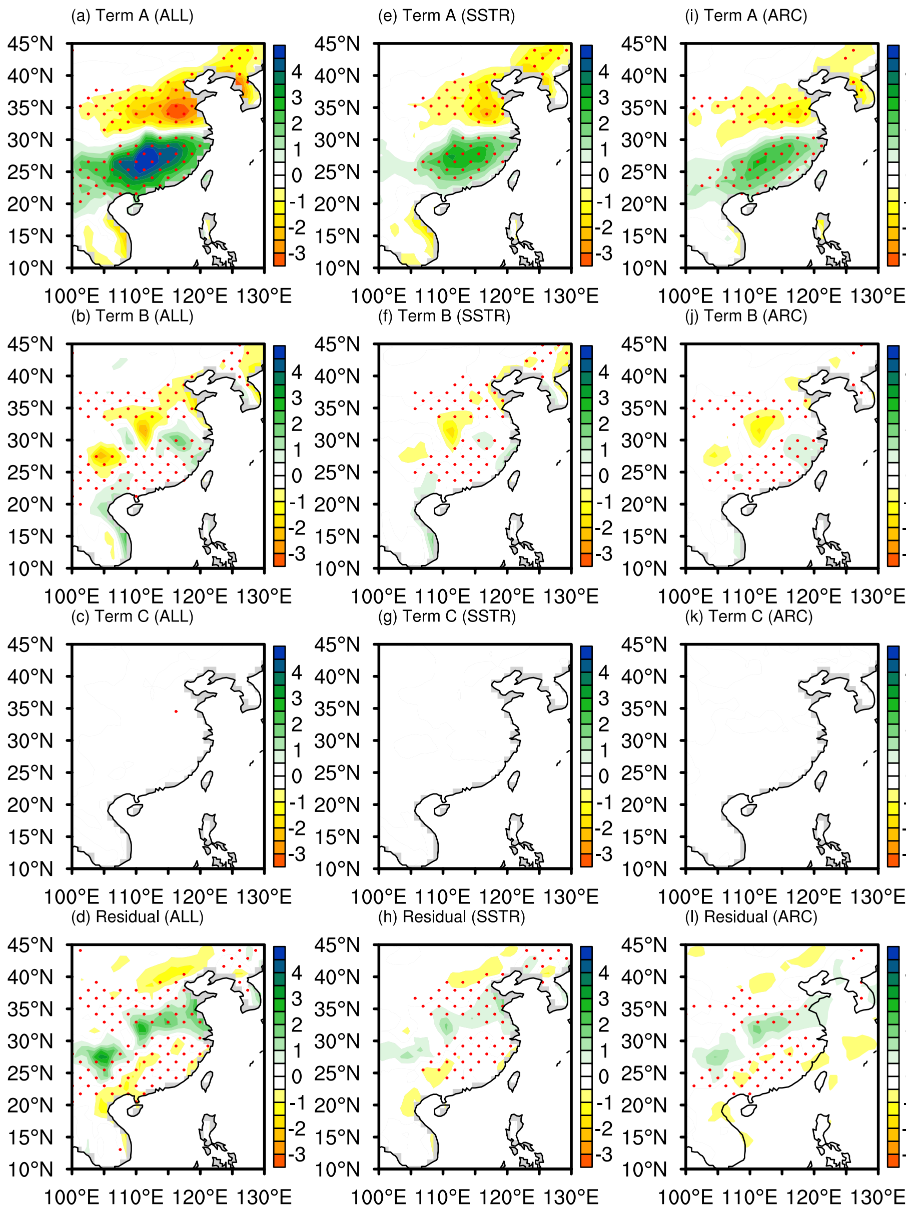

Supplementary Figure 4. Moisture processes driving changes in precipitation anomaly (July). The vertical transport differences of water vapor ($-<\omega\partial_p q>'$, units: mm day^{-1}) responses to ALL (a), SSTR (e) and ARC (i). The horizontal transport differences of water vapor ($-<\mathbf{V}_h \cdot \nabla_h q>'$, units: mm day^{-1}) responses to ALL (b), SSTR (f) and ARC (j). The evaporation (E', units: mm day^{-1}) responses to ALL (c), SSTR (g) and ARC (k). The residual (δ', units: mm day^{-1}) responses to ALL (d), SSTR (h) and ARC (l). Stippling indicates where the multi-model ensemble mean response is significant (90% confidence).

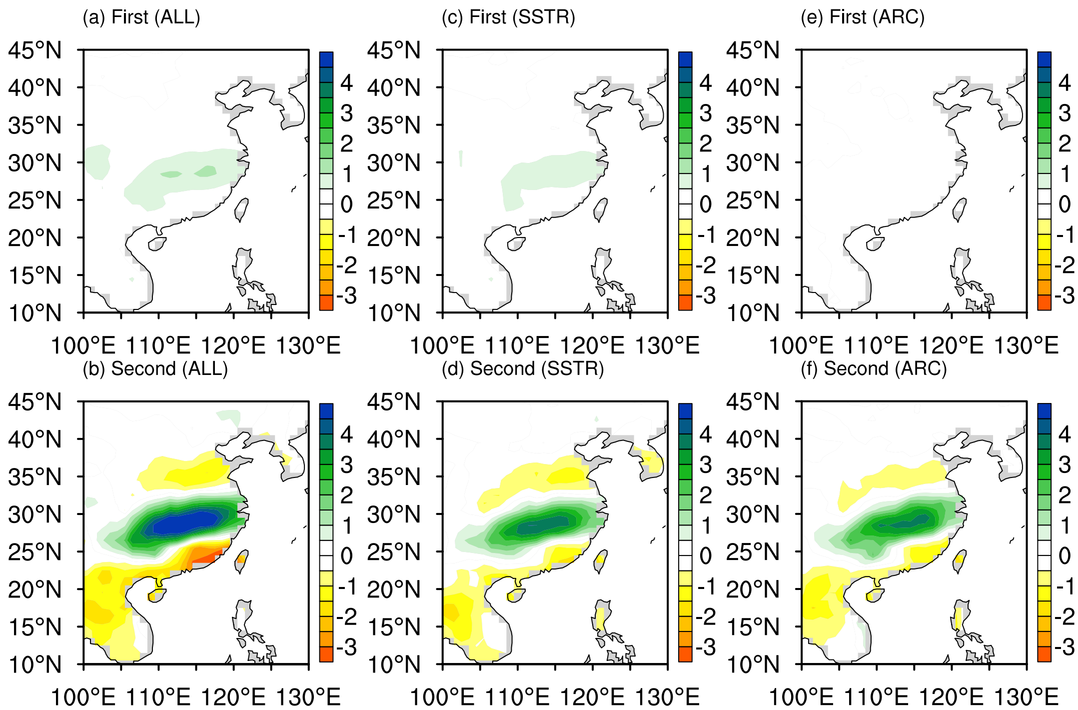

Supplementary Figure 5. Vertical moisture processes driving changes in precipitation anomaly (June). The response of the thermal term of vertical moisture advection ($-<\overline{\omega}\partial_p q'>$, units: mm day^{-1}) to ALL (a), SSTR (c), and ARC (e). The response of the dynamical term of vertical moisture advection ($-<\omega'\partial_p \overline{q}>$, units: mm day^{-1}) to ALL (b), SSTR (d), and ARC (f).

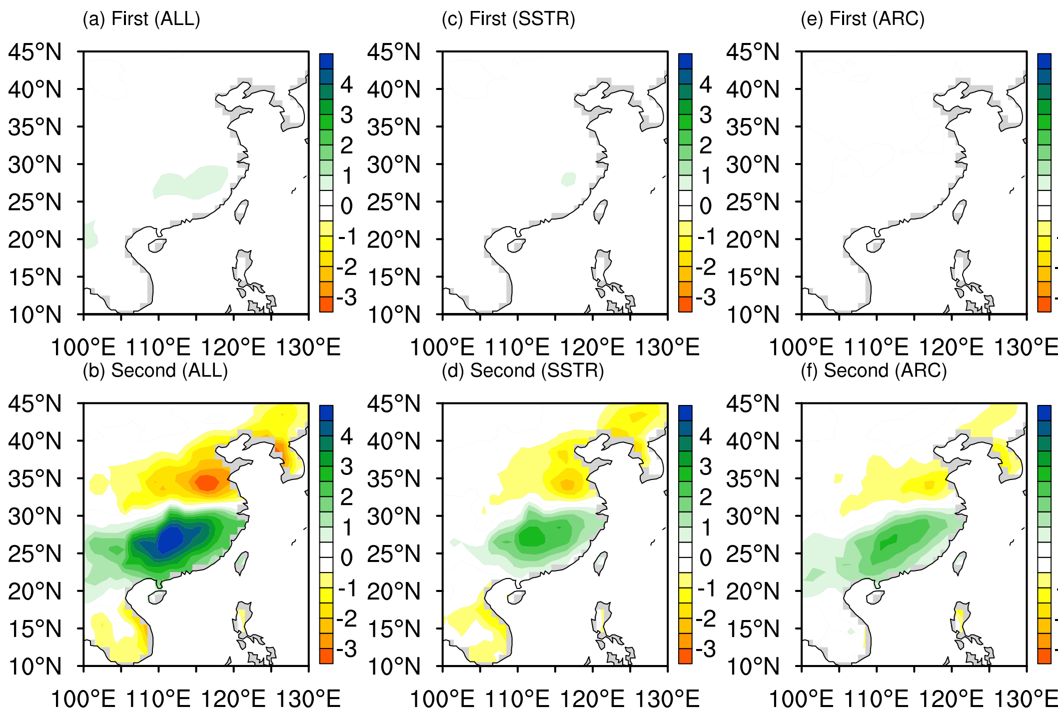

Supplementary Figure 6. Vertical moisture processes driving changes in precipitation anomaly (July). The response of the thermal term of vertical moisture advection ($-<\overline{\omega}\partial_p q'>$, units: mm day^{-1}) to ALL (a), SSTR (c), and ARC (e). The response of the dynamical term of vertical moisture advection ($-<\omega'\partial_p \overline{q}>$, units: mm day^{-1}) to ALL (b), SSTR (d), and ARC (f).

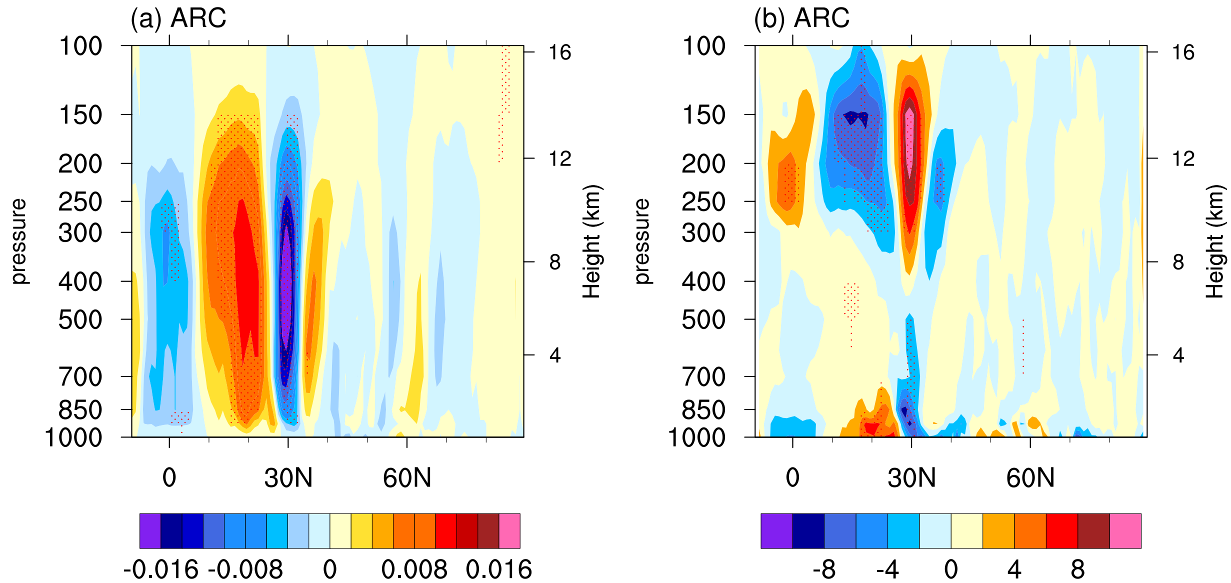

Supplementary Figure 7. Response of zonal-mean vertical velocity and divergence in June. Response of the zonal-mean (105ºE-135ºE) vertical velocity (a) (shading, units: Pa s^{-1}) and divergence (b) (shading, units: 10^6 s^{-1}) to the ARC in June. Stippling indicates where the multi-model ensemble mean response is significant (90% confidence).

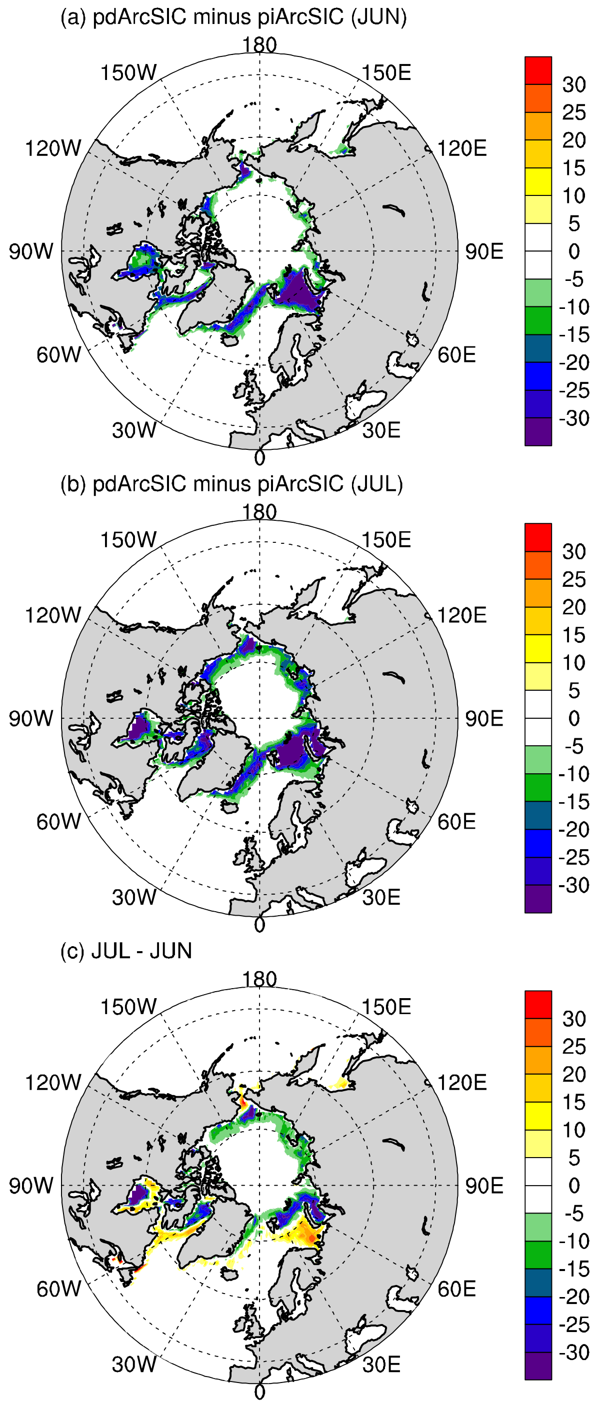

Supplementary Figure 8. The difference in Arctic sea ice concentration between present-day (pd) and pre-industrial (pi). The difference (shading, units: %) between present-day (pd) Arctic sea ice concentration and pre-industrial (pi) Arctic sea ice concentration in June (a) and July (b). Figure (c) shows the difference (shading, units: %) between Figure (a) and (b).

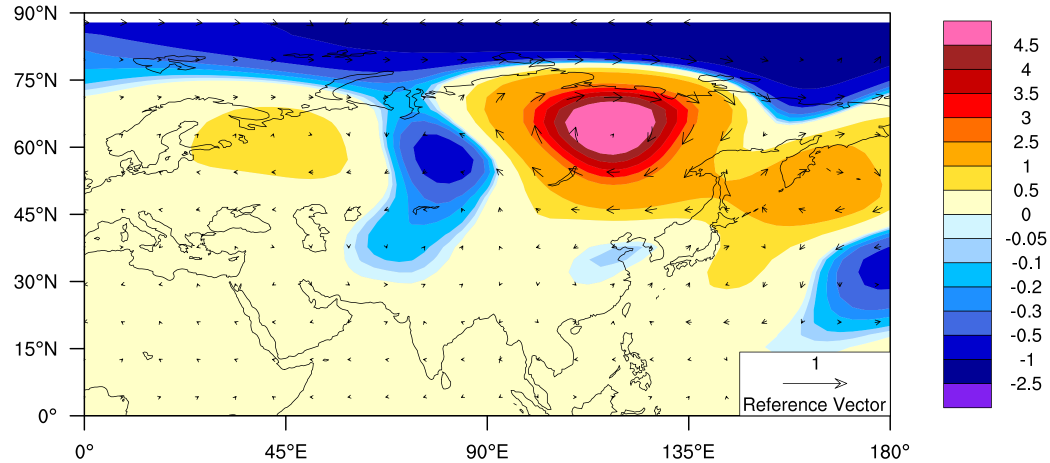

Supplementary Figure 9. Response to atmospheric heating. The 200 hPa geopotential height (contours; m) and wind (vectors; m s^{-1}) response to the atmospheric heating in WBS for Day 15 to Day 30.

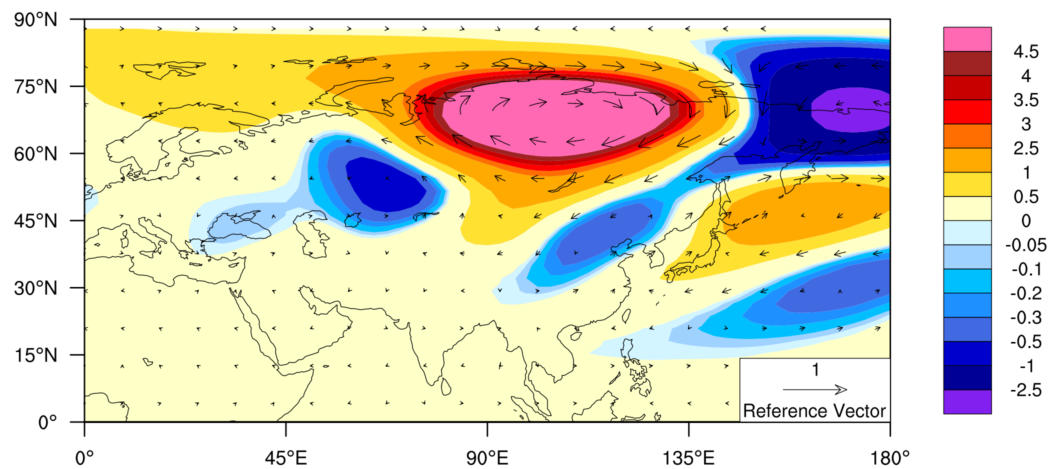

Supplementary Figure 10. Response to atmospheric heating. The 200 hPa geopotential height (contours; m) and wind (vectors; m s^{-1}) response to the atmospheric heating in WGB for Day 15 to Day 30.

Supplementary Table 1. Introduction to the models and experiments used in the research. The numbers in parentheses represent the number of ensemble members.

Model	Resolution	Experiment
HadGEM3-GC31-MM	324×432	piSST-piSIC(149) piSST-pdSIC(150) pdSST-piArcSIC(300) pdSST-pdSIC(300)
FGOALS-f3-L	180×288	piSST-piSIC(100) piSST-pdSIC(100) pdSST-piArcSIC(100) pdSST-pdSIC(100)
CESM2	192×288	piSST-piSIC(100) piSST-pdSIC(100) pdSST-piArcSIC(100) pdSST-pdSIC(100)
AWI-CM-1-1-MR	192×384	piSST-piSIC(100) piSST-pdSIC(100) pdSST-piArcSIC(100) pdSST-pdSIC(100)
CanESM5	64×128	piSST-piSIC(100) piSST-pdSIC(100) pdSST-piArcSIC(100) pdSST-pdSIC(100)
IPSL-CM6A-LR	143×144	piSST-piSIC(200) piSST-pdSIC(200) pdSST-piArcSIC(200) pdSST-pdSIC(200)

Supplementary Table 2. Introduction to LBM experiments

Number	Experiments	Description
NO.1	WBS (warming anomaly over the Barents Sea)	The forcing is horizontally elliptical and centered at 35°E, 70°N. The radius is 15° in longitude and 10° in latitude. The maximum amplitude of the forcing is at the lowest level. Basic state is June in the pdSST-pdSIC experiment.
NO.2	WBNR (Warm anomaly over the Barents Sea and North Coast of Russia)	The one forcing is horizontally elliptical and centered at 35°E, 70°N. The radius is 15° in longitude and 10° in latitude. Another forcing is horizontally elliptical and centered at 125°E, 75°N. The radius is 10° in longitude and 5° in latitude. The maximum amplitude of the forcing is at the lowest level. Basic state is July in the pdSST-pdSIC experiment.

Supplementary Table 3. The first 100 ensembles obtained by ranking the skill of the spatial correlations.

Model	Ensemble (JUN)	Ensemble (JUL)
HadGEM3-GC31-MM	r100i1p1f2 r10i1p1f2 r117i1p1f2 r125i1p1f2 r12i1p1f2 r130i1p1f2 r146i1p1f2 r22i1p1f2 r26i1p1f2 r36i1p1f2 r37i1p1f2 r3i1p1f2 r4i1p1f2 r52i1p1f2 r57i1p1f2 r70i1p1f2 r75i1p1f2 r79i1p1f2 r80i1p1f2	r126i1p1f2 r131i1p1f2 r134i1p1f2 r139i1p1f2 r64i1p1f2 r80i1p1f2 r81i1p1f2
FGOALS-f3-L	r19i1p1f1 r48i1p1f1 r49i1p1f1 r72i1p1f1 r89i1p1f1 r90i1p1f1 r94i1p1f1	r13i1p1f1 r17i1p1f1 r21i1p1f1 r26i1p1f1 r43i1p1f1 r48i1p1f1 r56i1p1f1 r62i1p1f1 r64i1p1f1 r71i1p1f1 r73i1p1f1 r77i1p1f1 r82i1p1f1 r85i1p1f1 r98i1p1f1

CESM2	r20i1p1f1 r22i1p1f1 r24i1p1f1 r30i1p1f1 r34i1p1f1 r4i1p1f1 r53i1p1f1 r62i1p1f1 r66i1p1f1 r74i1p1f1 r75i1p1f1 r7i1p1f1 r84i1p1f1 r88i1p1f1 r8i1p1f1 r92i1p1f1 r95i1p1f1 r97i1p1f1 r98i1p1f1	r22i1p1f1 r26i1p1f1 r28i1p1f1 r42i1p1f1 r52i1p1f1 r57i1p1f1 r68i1p1f1 r72i1p1f1 r74i1p1f1 r7i1p1f1 r81i1p1f1 r84i1p1f1 r87i1p1f1 r95i1p1f1 r9i1p1f1
AWI-CM-1-1-MR	r100i1p1f1 r12i1p1f1 r16i1p1f1 r2i1p1f1 r42i1p1f1 r52i1p1f1 r56i1p1f1 r58i1p1f1 r73i1p1f1 r74i1p1f1 r75i1p1f1 r81i1p1f1 r93i1p1f1 r98i1p1f1 r9i1p1f1	r13i1p1f1 r21i1p1f1 r23i1p1f1 r25i1p1f1 r26i1p1f1 r28i1p1f1 r44i1p1f1 r45i1p1f1 r49i1p1f1 r57i1p1f1 r59i1p1f1 r64i1p1f1 r65i1p1f1 r67i1p1f1 r75i1p1f1 r77i1p1f1 r7i1p1f1 r80i1p1f1 r84i1p1f1 r85i1p1f1 r8i1p1f1 r90i1p1f1

CanESM5	r24i1p2f1 r30i1p2f1 r31i1p2f1 r67i1p2f1 r75i1p2f1 r83i1p2f1 r88i1p2f1 r94i1p2f1 r97i1p2f1	r10i1p2f1 r14i1p2f1 r19i1p2f1 r22i1p2f1 r25i1p2f1 r26i1p2f1 r41i1p2f1 r46i1p2f1 r49i1p2f1 r52i1p2f1 r56i1p2f1 r58i1p2f1 r61i1p2f1 r64i1p2f1 r68i1p2f1 r73i1p2f1 r83i1p2f1 r86i1p2f1 r87i1p2f1 r89i1p2f1 r8i1p2f1 r93i1p2f1 r96i1p2f1 r9i1p2f1

	r101i1p1f1	
	r109i1p1f1	
	r110i1p1f1	
	r120i1p1f1	
	r123i1p1f1	
	r124i1p1f1	
	r139i1p1f1	
	r154i1p1f1	r10i1p1f1
	r155i1p1f1	r119i1p1f1
	r15i1p1f1	r121i1p1f1
	r161i1p1f1	r124i1p1f1
	r173i1p1f1	r127i1p1f1
	r176i1p1f1	r129i1p1f1
	r178i1p1f1	r130i1p1f1
	r181i1p1f1	r184i1p1f1
IPSL-CM6A-LR	r185i1p1f1	r192i1p1f1
	r26i1p1f1	r21i1p1f1
	r30i1p1f1	r2i1p1f1
	r34i1p1f1	r34i1p1f1
	r39i1p1f1	r3i1p1f1
	r42i1p1f1	r52i1p1f1
	r57i1p1f1	r68i1p1f1
	r5i1p1f1	r72i1p1f1
	r64i1p1f1	r89i1p1f1
	r68i1p1f1	
	r6i1p1f1	
	r70i1p1f1	
	r73i1p1f1	
	r74i1p1f1	
	r94i1p1f1	
	r97i1p1f1	